Articles

Structure and Facile Unimolecular Twist-Rotation of *cis*-Bis(silyl)bis(phosphine)platinum and *cis*-Bis(stannyl)bis(phosphine)palladium Complexes

Yasushi Tsuji,* Kayo Nishiyama, Sei-ichi Hori, Masahiro Ebihara, and Takashi Kawamura

Department of Chemistry, Faculty of Engineering, Gifu University, Gifu 501-1112, Japan

Received November 3, 1997

The structures and fluxional behavior of two *cis*-bis(silyl)bis(phosphine)platinum complexes (**2**), *cis*-[Pt(SiPh$_2$Me)$_2$(PMe$_2$Ph)$_2$] (**2a**) and *cis*-[Pt(SiFMe$_2$)$_2$(PEt$_3$)$_2$] (**2b**), and two *cis*-bis(stannyl)bis(phosphine)palladium complexes (**3**), *cis*-[Pd(SnMe$_3$)$_2$(PMe$_3$)$_2$] (**3a**) and *cis*-[Pd(SnMe$_3$)$_2$(PMePh$_2$)$_2$] (**3b**), were examined. The molecular structures of **2a** and **3a** were determined by X-ray crystallographic analysis. The complexes have twisted square-planar structures with *cis*-orientation of the ligands. The bis(silyl)platinum complexes, **2a** and **2b**, show fluxional behavior on the NMR time scale. In the fluxional process, the spin−spin coupling between P, Si, and Pt is retained; namely these nuclear spin states are intramolecularly conserved. The fluxionality of **2a** and **2b** is attributed to unimolecular twist-rotation via a pseudotetrahedral transition state. Similar fluxionality of the bis(stannyl)palladium complex, **3b**, is evident by utilizing both solution- and solid-state ^{31}P NMR.

Introduction

The structure and reactivity of transition-metal silyl[1] and stannyl[2] complexes are of recent interest, and theoretical studies[3] of these complexes in some catalytic cycles have also been carried out. We recently reported the fluxional behavior of *cis*-bis(stannyl)bis(phosphine)-platinum complexes (**1**) and proposed that the unimolecular twist-rotation is responsible for the fluxionality on the basis of NMR measurement and ab initio molecular orbital calculations.[4]

In this paper, we report that the fluxionality is not limited to **1** but is also observed for *cis*-bis(silyl)bis(phosphine)platinum (**2**) and *cis*-bis(stannyl)bis(phosphine)palladium complexes (**3**) on the basis of X-ray crystallographic analysis and multinuclear NMR measurements (^{31}P, ^{29}Si, and ^{119}Sn including solid-state CPMAS ^{31}P), Chart 1. These bis(silyl) (**2**) and bis(stannyl) (**3**) complexes are implicated as important active catalyst species in a number of transition-metal-catalyzed silylation[5] and stannylation[6] reactions using organodisilanes and -distannanes.

(1) (a) Ozawa, F.; Hikida, T. *Organometallics* **1996**, *15*, 4501. (b) Ozawa, F.; Hikida, T. *J. Am. Chem. Soc.* **1994**, *116*, 2844. (c) Schubert, U.; Gilges, H. *Organometallics* **1996**, *15*, 2373. (d) Shimada, S.; Tanaka, M.; Honda, K. *J. Am. Chem. Soc.* **1995**, *117*, 8289. (e) Xue, Z.; Li, L.; Hoyt, L. K.; Diminnie, J. B.; Pollitte, J. L. *J. Am. Chem. Soc.* **1994**, *116*, 2169. (f) Richard, C. E. F.; Roper, W. R.; Salter, D. M.; Wright, L. J. *J. Am. Chem. Soc.* **1992**, *114*, 9682. (g) Lichtenberger, D. L.; Rai-Chaudhuri, A. *J. Am. Chem. Soc.* **1991**, *113*, 2923. (h) Kirchgaessner, U.; Piana, H.; Schubert, U. *J. Am. Chem. Soc.* **1991**, *113*, 2228.

(2) (a) Schubert, U.; Grubert, S. *Organometallics* **1996**, *15*, 4707. (b) Seebald, S.; Mayer, B.; Schubert, U. *Inorg. Chem.* **1995**, *34*, 5285. (c) Schubert, U.; Mayer, B.; Russ, C. *Chem. Ber.* **1994**, *127*, 2189. (d) Chipperfield, J. R.; Clark, S.; Webster, D. E.; Yusof, H. *J. Organomet. Chem.* **1991**, *421*, 205.

(3) (a) Sakaki, S.; Ogawa, M.; Musashi, Y.; Arai, T. *J. Am. Chem. Soc.* **1994**, *116*, 7258. (b) Hada, M.; Tanaka, Y.; Ito, M.; Murakami, M.; Amii, H.; Ito, Y.; Nakatsuji, H. *J. Am. Chem. Soc.* **1994**, *116*, 8754.

(4) Obora, Y.; Tsuji, Y.; Nishiyama, Y.; Ebihara, M.; Kawamura, T. *J. Am. Chem. Soc.* **1996**, *118*, 10922.

(5) (a) Tsuji, Y.; Lago, R. M.; Tomohiro, S.; Tsuneishi, H. *Organometallics* **1992**, *11*, 2353. (b) Tsuji, Y.; Funato, M.; Ozawa, M.; Ogiyama, H.; Kajita, S.; Kawamura, T. *J. Org. Chem.* **1996**, *61*, 5779. (c) Obora, Y.; Tsuji, Y.; Kawamura, T. *J. Am. Chem. Soc.* **1993**, *115*, 10414. (d) Obora, Y.; Tsuji, Y.; Kawamura, T. *J. Am. Chem. Soc.* **1995**, *117*, 9814. (e) Murakami, M.; Sugimome, M.; Fujimoto, K.; Nakamura, H.; Anderson, P. G.; Ito, Y. *J. Am. Chem. Soc.* **1993**, *115*, 6487. (f) Ito, Y.; Suginome, M.; Murakami, M. *J. Org. Chem.* **1991**, *56*, 1948. (g) Yamashita, H.; Catellani, M.; Tanaka, M. *Chem. Lett.* **1991**, 241. (h) Sakurai, H.; Eriyama, Y.; Kamiyama, Y.; Nakadaira, Y. *J. Organomet. Chem.* **1984**, *264*, 229. (i) Carlson, C. W.; West, R. *Organometallics* **1983**, *2*, 1801. (j) Watanabe, H.; Kobayashi, M.; Saito, M.; Nagai, Y. *J. Organomet. Chem.* **1981**, *216*, 149. (k) Watanabe, H.; Kobayashi, M.; Higuchi, K.; Nagai, Y. *J. Organomet. Chem.* **1980**, *186*, 51. (l) Matsumoto, H.; Matsubara, I.; Kato, T.; Shono, K.; Watanabe, H.; Nagai, Y. *J. Organomet. Chem.* **1980**, *199*, 43. (m) Matsumoto, H.; Shono, K.; Wada, A.; Matsubara, I.; Watanabe, H.; Nagai, Y. *J. Organomet. Chem.* **1980,** *199*, 185. (n) Tamao, K.; Okazaki, S.; Kumada, M. *J. Organomet. Chem.* **1978**, *146*, 87. (o) Tamao, K.; Hayashi, T.; Kumada, M. *J. Organomet. Chem.* **1976**, *114*, C19. (p) Sakurai, H.; Kamiyama, Y.; Nakadaira, Y. *Chem. Lett.* **1975**, 887. (q) Sakurai, H.; Kamiyama, Y.; Nakadaira, Y. *J. Am. Chem. Soc.* **1975**, *97*, 931. (r) Okinoshima, H.; Yamamoto, K.; Kumada, M. *J. Am. Chem. Soc.* **1972**, *94*, 9263. (s) Hatanaka, Y.; Hiyama, T. *Tetrahedron Lett.* **1987**, *28*, 4715.

(6) (a) Tsuji, Y.; Kakehi, T. *J. Chem. Soc., Chem. Commun.* **1992**, 1000. (b) Obora, Y.; Tsuji, Y.; Kakehi, T.; Kobayashi, M.; Shinkai, Y.; Ebihara, M.; Kawamura, T. *J. Chem. Soc., Perkin Trans. 1* **1995**, 599. (c) Obora, Y.; Tsuji, Y.; Asayama, M.; Kawamura, T. *Organometallics* **1993**, *12*, 4697. (d) Piers, E.; Skerlj, R. T *J. Org. Chem.* **1987**, *52*, 4421. (e) Mitchell, T. N.; Schneider, U. *J. Organomet. Chem.* **1991**, *407*, 319.

S0276-7333(97)00957-6 CCC: $15.00
Publication on Web 01/17/1998

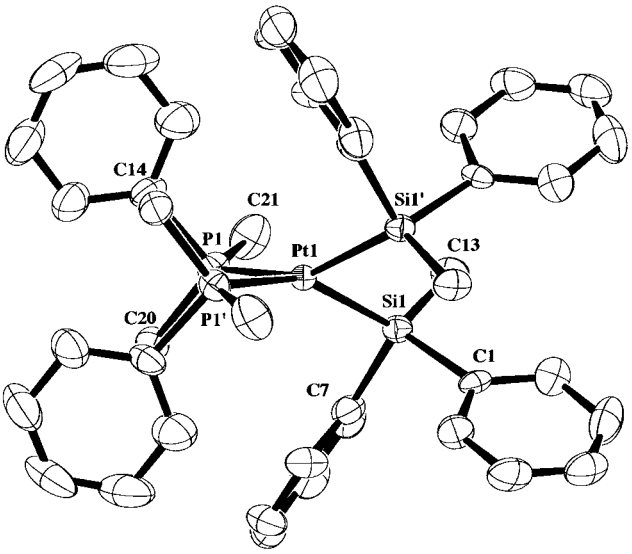

Figure 1. Perspective ORTEP drawing of the molecular structure of complex **2a**. All non-hydrogen atoms are represented by thermal ellipsoids drawn to encompass 50% probability, and hydrogen atoms are deleted for ease of viewing.

Chart 1

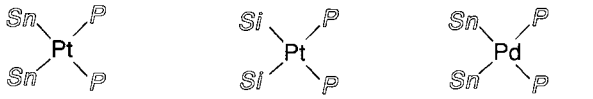

Sn: stannyl
P : phosphine

Si: silyl
P : phosphine

Sn: stannyl
P : phosphine

1 **2** **3**

Table 1. Selected Bond Distances and Angles for 2a

	Distances (Å)		
Pt(1)−P(1)	2.352(2)	Pt(1)−Si(1)	2.359(2)
P(1)−C(14)	1.821(7)	P(1)−C(20)	1.815(7)
P(1)−C(21)	1.813(9)	Si(1)−C(1)	1.911(6)
Si(1)−C(7)	1.913(7)	Si(1)−C(13)	1.885(7)
	Angles (deg)		
P(1)−Pt(1)−P(1′)	96.48(10)	Si(1)−Pt(1)−Si(1′)	88.91(9)
P(1)−Pt(1)−Si(1)	93.69(6)	P(1)−Pt(1)−Si(1′)	152.42(7)
Pt(1)−P(1)−C(14)	108.5(2)	Pt(1)−P(1)−C(20)	124.3(3)
Pt(1)−P(1)−C(21)	115.9(3)	Pt(1)−Si(1)−C(1)	113.5(2)
Pt(1)−Si(1)−C(7)	105.0(2)	Pt(1)−Si(1)−C(13)	123.4(2)

Results and Discussion

Structure and Fluxional Behavior of *cis*-Bis(silyl)bis(phosphine)platinum (2). *cis*-[Pt($SiPh_2$-$Me)_2(PMe_2Ph)_2$] (**2a**) was prepared by the method reported by Chatt *et al.*[7] using the corresponding dichloroplatinum complex and the silyllithium. Since no X-ray structure of **2a** was available, an X-ray diffraction study was carried out. The molecular structure of **2a** is shown in Figure 1. Table 1 lists selected bond distances and angles for **2a**. The complex has a twisted square-planar structure with *cis*-orientation of the ligands. The structure is distinctly distorted from planarity; the dihedral angle between the PtP_2 and the $PtSi_2$ plane is 38.1°. The steric congestion associated with the substituents on the P and the Si atoms may cause the distortion from the planarity.

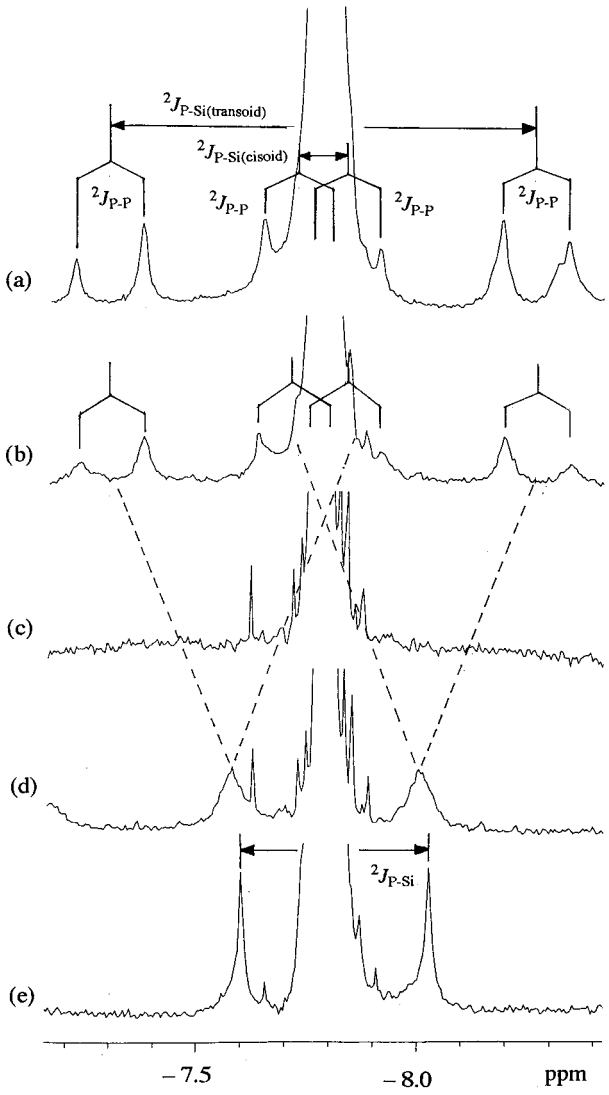

Figure 2. ^{31}P NMR spectra (central part) of **2a** in CD_2Cl_2 (162 MHz) at (a) − 70 °C, (b) − 30 °C, (c) − 10 °C, (d) 10 °C, and (e) 30 °C.

The $^{31}P\{^1H\}$ NMR spectra of **2a** were measured at various temperatures and are shown in Figure 2. The spectrum at −70 °C (Figure 2a) showed resonances centered at −7.8 ppm with the satellite peaks due to $^2J_{P-Si(transoid)}$ (156 Hz), $^2J_{P-Si(cisoid)}$ (18 Hz), and $^2J_{P-P}$ (24 Hz); only the central part of the spectrum is shown in the figure, omitting satellite peaks due to $^1J_{P-Pt}$ coupling. On warming, the satellite peaks due to $^2J_{P-Si(transoid)}$ and $^2J_{P-Si(cisoid)}$ became broad at −30 °C (Figure 2b) and coalesced at −10 °C (Figure 2c) while the *sharp* main resonance was maintained. The satellite peaks reappeared as broad resonances at 10 °C (Figure 2d) and sharpened at 30 °C (Figure 2e) with an averaged $^2J_{P-Si}$ value (69 Hz).[8] This fluxional process is reversible, and throughout the process the $^1J_{P-Pt}$ value is maintained; $^1J_{P-Pt}$ = 1572 Hz at −70 °C, 1570 Hz at −30 °C, 1566 Hz at −10 °C, 1560 Hz at 10 °C, and 1557 Hz at 30 °C. The thermodynamic parameters

(7) (a) Chatt. J.; Eaborn, C.; Ibekwe, S. D.; Kapoor, P. N. *J. Chem. Soc. A* **1970**, 1343. (b) Eaborn, C.; Metham, T. N.; Pidcock, A. *J. Chem. Soc., Dalton Trans.* **1975**, 2212. (c) Eaborn, C.; Pidcock, A.; Ratcliff, B. *J. Organomet. Chem.* **1974**, *66*, 23.

(8) This values are equal to $(|^2J_{P-Si(transoid)}| - |^2J_{P-Si(cisoid)}|)/2$, indicating $^2J_{P-Si(transoid)}$ and $^2J_{P-Si(cisoid)}$ are of opposite sign.

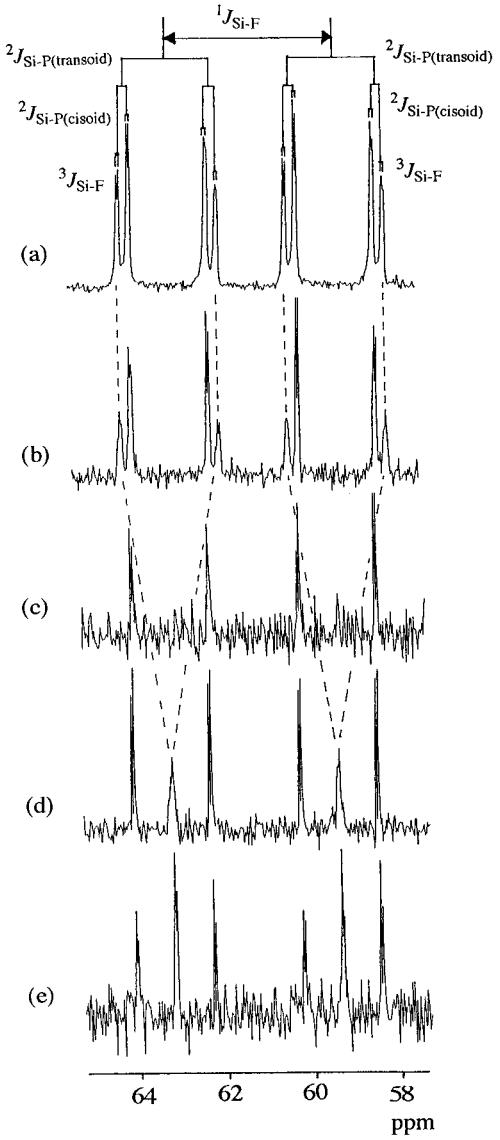

Figure 3. ^{29}Si NMR spectra (central part) of **2b** in toluene-d_8 (79.3 MHz) at (a) − 80 °C, (b) − 50 °C, (c) − 30 °C, (d) 20 °C, and (e) 40 °C.

were obtained by simulating the spectra: $\Delta H = 57 \pm 2$ kJ mol^{-1} and $\Delta S = 17 \pm 9$ J mol^{-1} K^{-1}.

The fluxional behavior of **2** is further distinct using *cis*-[Pt(SiFMe$_2$)$_2$(PEt$_3$)$_2$] (**2b**).[9] The fluxional process of **2b** was examined with ^{29}Si{^{1}H} NMR at various temperatures (Figure 3). At −80 °C (Figure 3a), the resonances (61.2 ppm) appeared as two sets of ddd with $^1J_{Si-F} = 300$ Hz, $^2J_{Si-P(transoid)} = 157$ Hz, $^2J_{Si-P(cisoid)} = 19$ Hz, and $^3J_{Si-F} = 3.9$ Hz; satellite peaks due to $^1J_{Si-Pt}$ are omitted in the figure. With an increase in the temperature, only the outer resonances of each set became broad at −50 °C (Figure 3b) and collapsed at −30 °C (Figure 3c). The resonances reappeared as broad peaks at 20 °C (Figure 3d) and then sharpened at 40 °C (Figure 3e), at the midpoint of the resonances, with $^1J_{Si-F} = 302$ Hz, $^2J_{Si-P} = 69$ Hz,[8] and $^3J_{Si-F} = 3.9$ Hz. In the meantime, the inner lines remained sharp with constant separation: $[|^2J_{Si-P(transoid)}| - |^2J_{Si-P(cisoid)}|]$. The inner lines are assigned to ^{29}Si transitions associated with the phosphorus spin states $\alpha\alpha$ and $\beta\beta$, while the collapsing (outer) lines are assigned to transitions with the phosphorus spin states $\alpha\beta$ and $\beta\alpha$. This behavior also indicates that $^2J_{P-Si(transoid)}$ and $^2J_{P-Si(cisoid)}$ have opposite signs. The fluxional process is reversible, and throughout the process the $^1J_{P-Pt}$ is maintained; $^1J_{P-Pt} = 1243$ Hz at −80 °C, 1250 Hz at −50 °C, 1252 Hz at −30 °C, 1267 Hz at 20 °C, and 1269 Hz at 40 °C. By simulating the spectra, the following activation parameters were obtained: $\Delta H = 34 \pm 1$ kJ mol^{-1} and $\Delta S = -60 \pm 6$ J mol^{-1}K^{-1}.

Scheme 1

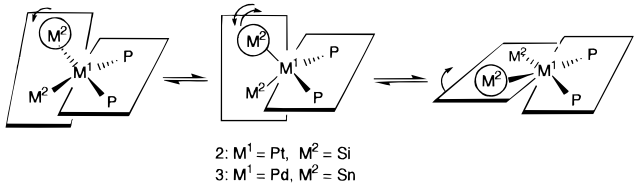

In these fluxional processes of **2a** and **2b**, the spin−spin coupling between the P, Si, and Pt nuclei is retained; namely, these nuclear spin states are intramolecularly conserved. Thus, within the limits of the NMR experiments,[10] a dissociative or consecutive displacement mechanism involving Pt−Si or Pt−P bond cleavage can be excluded. Analogous fluxional behavior was observed for *cis*-[PtH(SiR$_3$)(PPh$_3$)$_2$].[11] These features of the bis(silyl)platinum complexes (**2a**,**b**) are very reminiscent of the corresponding bis(stannyl)platinum complexes (**1**).[4] Ab initio molecular orbital calculations carried out for *cis*-Pt(SiH$_3$)$_2$(PH$_3$)$_2$ as a model complex suggest[12] that **2** and **1** have comparable activation energy for the twist-rotation, which is supported by the observed ΔH values for **2a** and **2b** (vide supra). Thus, we attribute the fluxionality of **2a** and **2b** to the similar unimolecular twist-rotation via a pseudotetrahedral transition state (Scheme 1).

Structure and Fluxional Behavior of *cis*-Bis(stannyl)bis(phosphine)palladium (3). The new *cis*-bis(stannyl)bis(phosphine)palladium complexes (**3a** and 3**b**) were prepared by oxidative addition of Me$_3$SnSnMe$_3$ to the corresponding palladium (0) phosphine complexes (**4a** and **4b**)[13] (eq 1) and obtained in analytically pure form. Noteworthy is that this is the first example of

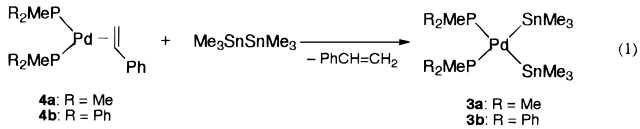

(1)

the oxidative addition of an Sn−Sn σ-bond to a palladium(0) phosphine complex, which is often employed as a catalyst precursor in bis(stannylation) reactions using organodistannanes. An X-ray crystallographic analysis was carried out for the trimethylphosphine complex (**3a**), and the molecular structure is shown in

(9) Yamashita, H.; Kobayashi, T.-a.; Hayashi, T.; Tanaka, M. *Chem. Lett.* **1990**, 1447.

(10) Jesson, J. P.; Muetterties, E. L. In *Dynamic Nuclear Magnetic Resonance Spectroscopy*; Jackman, L. M., Cotton, F. A., Eds; Academic: New York, 1975; p 256.

(11) Azizian, H.; Dixon, K. R.; Eaborn, C.; Pidcock, A.; Shuaib, N. M.; Vinaixa, J. *J. Chem. Soc., Chem. Commun.* **1982**, 1020.

(12) The detailed theoretical account of the unimolecular twist-rotation will be published in due course.

(13) Ozawa, F.; Son, T.; Ebina, S.; Osakada, K.; Yamamoto, A. *Organometallics*, **1992**, *11*, 171 and references therein.

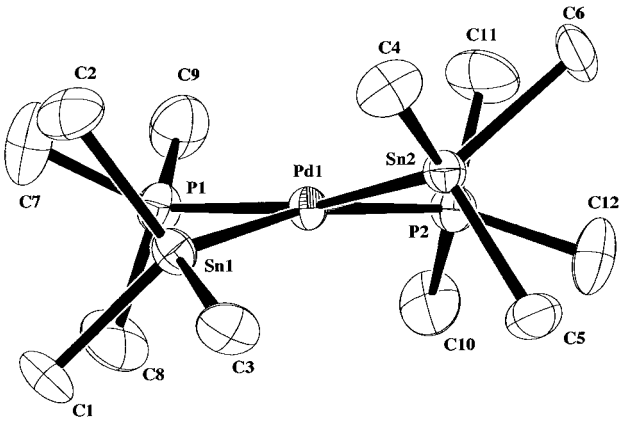

Figure 4. Perspective ORTEP drawing of the molecular structure of complex **3a**. All non-hydrogen atoms are represented by thermal ellipsoids drawn to encompass 50% probability, and hydrogen atoms are deleted for ease of viewing.

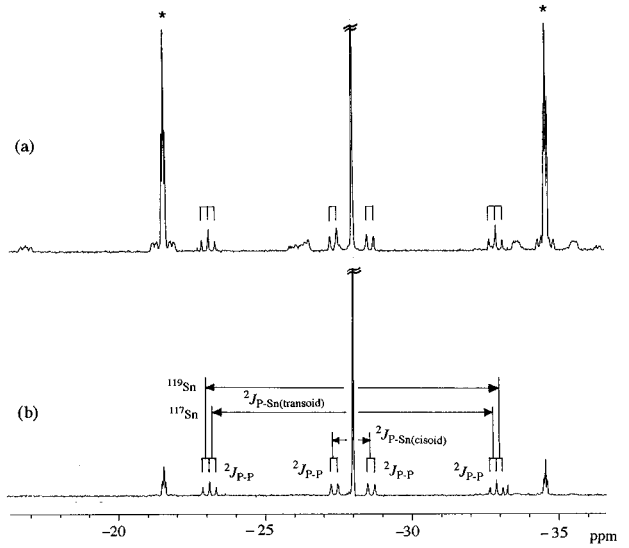

Figure 5. ^{31}P NMR spectra (central part) of **3a** in toluene-d_8 (162 MHz) at −90 °C; (a) without added $Me_3SnSnMe_3$, (b) with added $Me_3SnSnMe_3$: $[Me_3SnSnMe_3]/[\mathbf{3a}] = 2$.

Figure 4. Selected bond distances and angles for **3a** are listed in Table 2. Again, the complex has a twisted square-planar structure; the dihedral angle between the PdP_2 and the $PdSn_2$ plane is 16.8°.

The $^{31}P\{^1H\}$ NMR spectra of **3a** are shown in Figure 5. At −90 °C, $^{31}P\{^1H\}$ NMR resonances due to **3a** appeared as a sharp peak at −28.0 ppm (Figure 5a), while at room temperature, the resonances were broad (line width at half-height = 100 Hz) without any J couplings. Although the complex was analytically pure, two large unidentified resonances (marked with an asterisk (*) in the figure) appeared at −34.6 and −21.5 ppm having some J_{P-P} and J_{P-Sn} couplings; the ratio of the resonances at −34.6, −28.0, and −21.5 ppm is 1:1:1 at −90 °C (Figure 5a). The unidentified resonances may be assigned to a species formed by reductive elimination giving $Me_3SnSnMe_3$, since the $^{119}Sn\{^1H\}$ NMR spectrum of the same solution confirmed a comparable formation of $Me_3SnSnMe_3$ (−110.40 ppm, $^1J_{Sn-Sn} = 4165$ Hz; lit:[14] −108.7 ppm, $^1J_{Sn-Sn} = 4210$ Hz). Addition of 2 equiv of $Me_3SnSnMe_3$ to the solution reduced the unidentified resonances at −34.6 and −21.5 ppm and enhanced the resonance of **3a** (−28.0 ppm); the ratio between these resonances became 1:9:1 at −90 °C (Figure 5b). Irrespective of the absence or presence of the added $Me_3SnSnMe_3$, the resonance of **3a** at −28.0 ppm has $^2J_{P-Sn(transoid)}$ (1546 and 1618 Hz[15]), $^2J_{P-Sn(cisoid)}$ (203 Hz), and $^2J_{P-P}$ (38 Hz) couplings, which is consistent with the static *cis*-structure such that as shown in Figure 4.

Table 2. Selected Bond Distances and Angles for 3a

Distances (Å)			
Pd(1)−P(1)	2.337(3)	Pd(1)−Sn(1)	2.607(1)
P(1)−C(7)	1.84(1)	P(1)−C(8)	1.82(1)
P(1)−C(9)	1.86(1)	Sn(1)−C(1)	2.22(1)
Sn(1)−C(2)	2.19(1)	Sn(1)−C(3)	2.18(1)
Pd(1)−P(2)	2.323(3)	Pd(1)−Sn(2)	2.604(1)
P(2)−C(10)	1.83(1)	P(2)−C(11)	1.84(1)
P(2)−C(12)	1.84(1)	Sn(2)−C(4)	2.19(1)
Sn(2)−C(5)	2.17(1)	Sn(2)−C(6)	2.18(1)
Angles (deg)			
P(1)−Pd(1)−P(2)	98.1(1)	Sn(1)−Pd(1)−Sn(2)	80.71(3)
P(1)−Pd(1)−Sn(1)	91.62(8)	P(2)−Pd(1)−Sn(2)	91.91(8)
P(1)−Pd(1)−Sn(2)	165.95(9)	P(2)−Pd(1)−Sn(1)	164.77(9)
Pd(1)−P(1)−C(7)	117.0(5)	Pd(1)−P(1)−C(8)	117.1(5)
Pd(1)−P(1)−C(9)	116.6(4)	Pd(1)−Sn(1)−C(1)	112.8(4)
Pd(1)−Sn(1)−C(2)	115.5(4)	Pd(1)−Sn(1)−C(3)	123.8(3)
Pd(1)−P(2)−C(10)	113.3(4)	Pd(1)−P(2)−C(11)	116.0(5)
Pd(1)−P(2)−C(12)	120.8(5)	Pd(1)−Sn(2)−C(4)	121.5(3)
Pd(1)−Sn(2)−C(5)	114.4(3)	Pd(1)−Sn(2)−C(6)	113.5(3)

Because a fluxional behavior was not explicit with **3a**, a methyldiphenylphosphine complex (**3b**) was prepared (eq 1) and characterized. Judging from its $^{119}Sn\{^1H\}$ NMR spectrum, in contrast to **3a**, **3b** does not undergo reductive elimination giving $Me_3SnSnMe_3$. Therefore, the $^{31}P\{^1H\}$ NMR spectrum of **3b** is fairly simple, even without the added $Me_3SnSnMe_3$ (Figure 6), although the small unidentified peak (marked with an asterisk (*) in the figure) appeared. The ^{31}P resonance measured at −50 °C has satellite peaks due to $^2J_{P-Sn}$ (596 and 623 Hz)[15] (Figure 6a). Since the $^2J_{P-Sn}$ values are comparable to $(|^2J_{Sn-P(transoid)}| - |^2J_{Sn-P(cisoid)}|)/2$ calculated for **3a** (namely, 672 and 708 Hz, the averaged $^2J_{P-Sn}$ values), it is evident that **3b** undergoes a fluxional process and that the process is fast on the NMR time scale, even at −50 °C. On lowering the temperature, the satellite peak became broad at −80 °C (Figure 6b) and coalesced at −90 °C (Figure 6c) while the *sharp* main resonance was maintained. The fluxional process could not be frozen out in the solution state because of the freezing of the solvent and the limited solubility of the complex in other solvents of lower freezing point. However, solid-state CPMAS $^{31}P\{^1H\}$ NMR measured at 25 °C (Figure 6d) confirmed the static *cis*-structure of **3b**. In the spectrum, the satellite peak due to $^2J_{P-Sn(transoid)}$ (1650 Hz) appeared with a similar J value to those of **3a** (1546 and 1618 Hz, vide supra) whereas $^2J_{P-Sn(cisoid)}$ coupling (203 Hz for **3a**) may be buried in the broad main peak (line width at half-height = 300 Hz). Thus, the fluxional behavior of **3b** is evident by utilizing both solution- and solid-state ^{31}P NMR. The fluxional process of **3b**, in which the P and Sn spin

(14) Mitchell, T. N.; Walter, G. *J. Chem. Soc., Perkin Trans. 2* **1977**, 1842.

(15) The ratio of the coupling constants is equal to that of the gyromagnetic ratio[15a] of ^{117}Sn and ^{119}Sn. (a) Brevard, C.; Granger, P. *Handbook of High-Resolution Multinuclear NMR*; John Wiley & Sons: New York, 1981; p 168.

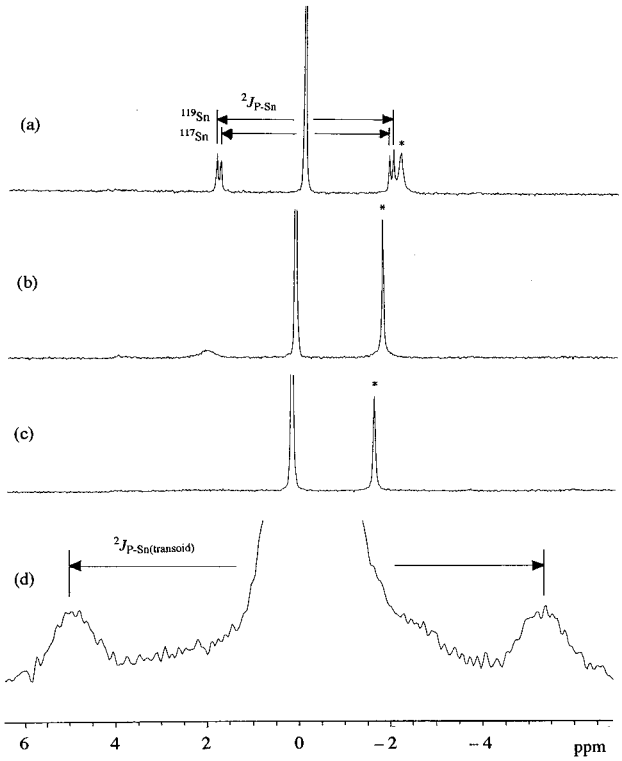

Figure 6. ^{31}P NMR spectra (central part) of **3b** in toluene-d_8 (162 MHz) at (a) − 50 °C, (b) − 80 °C, and (c) − 90 °C and (d) solid-state CPMAS spectrum (162 MHz) at 25 °C.

states are conserved, may be explained analogously by the unimolecular twist rotation depicted in Scheme 1.

Experimental Section

General Procedure and Materials. All manipulations of air-sensitive materials were performed under an argon atmosphere in conventional Schlenk-type glassware on a dual-manifold Schlenk line or in a nitrogen-filled glovebox (UNICO, UN-650F). NMR spectra were recorded on a JEOL α-400 (solution; ^{31}P 162 MHz, ^{29}Si 79.3 MHz, and ^{119}Sn 149 MHz) or a Varian Inova-400 (CPMAS; ^{31}P 162 MHz). Solution NMR measurements on air-sensitive samples were conducted in Teflon-valve-sealed tubes (J. Young). The ^{29}Si NMR measurement was carried out with an INEPT pulse sequence. CPMAS ^{31}P NMR was measured at a 7.5 kHz rotational frequency at room temperature. Chemical shifts are referred to external 85% H_3PO_3 for ^{31}P, Me_4-Si for ^{29}Si, or Me_4Sn for ^{119}Sn. Elemental analysis was performed at the Microanalytical Center of Kyoto University.

The reagents and solvents were dried and purified by the usual procedures.[16] Deuterated solvents were degassed and vacuum-transferred onto 4 Å molecular sieves before use. 1,2-Difluorotetramethyldisilane,[17] hexamethyldistannane,[18] $Pt(PEt_3)_3$,[19] **2a**,[7] **2b**,[9] and **4a,b**[13] were prepared by the literature methods.

(16) Perrin, D. D.; Armagego, W. L. F. *Purification of Laboratory Chemicals*, 3rd ed.; Pergamon: Oxford, 1988.
(17) Kumada, M.; Yamaguchi, M.; Yamamoto, Y.; Nakajima, J.; Shiina, K. *J. Org. Chem.* **1956**, *21*, 1264.
(18) Smith, G. F.; Kuivila, H. G.; Simon, R.; Sultan, L. *J. Am. Chem. Soc.* **1981**, *103*, 833.
(19) Yoshida, T.; Matsuda, T.; Otsuka, S. *Inorg. Synth.* **1979**, *19*, 110.

Table 3. Summary of Crystal Structure Data for Complexes 2a and 3a[a]

complex	**2a**	**3a**
formula	$C_{42}H_{48}P_2PtSi_2$	$C_{12}H_{36}P_2PdSn_2$
fw	866.05	586.14
data collectn T, °C	−74.0	−60.0
cryst system	monoclinic	orthorhombic
space group	*C*2/*c* (No. 15)	*Pbca* (No. 61)
a, Å	15.449(2)	12.047(3)
b, Å	14.601(3)	36.416(8)
c, Å	17.787(2)	9.768(3)
β, deg	105.427(8)	
V, Å^3	3867.8(9)	4285(1)
Z	4	8
d_{calcd}, g cm^{-3}	1.487	1.817
cryst size, mm	0.15 × 0.15 × 0.05	0.40 × 0.20 × 0.10
habit	prismatic	prismatic
μ, cm^{-1}	38.01	32.79
transmission factors	0.8026−1.0000	0.6767−1.0000
intensities (unique, R_i)	4789 (4616, 0.048)	5533 (5533)
intensities > 3.00$\sigma(I)$	3053	3084
number of params	213	154
R^b	0.039	0.047
$R_w{}^b$	0.042	0.057
GOF	1.03	1.61

[a] Radiation, graphite-monochromated, Mo Kα, λ = 0.710 69 Å; scan type $\omega-2\theta$; $2\theta_{max}$ = 55.0°. [b] $R = \sum||F_o| - |F_c||/\sum|F_o|$, $R_w = [(\sum w(|F_o| - |F_c|)^2/\sum wF_o^2)]^{1/2}$, $w = [\sigma^2(F_o) + 0.0001F_o^2]^{-1}$.

Preparation of 3a. In a 100 mL flask, distilled styrene (0.687 g, 6.60 mmol) was degassed by three freeze−pump−thaw sequences and toluene (15 mL) was vacuum-transferred on it. In a glovebox filled with dry N_2, $PdEt_2(PMe_3)_2$ (0.603 g, 1.90 mmol) was added to the solution. The mixture was stirred at 55 °C for 2 h to afford $Pd(styrene)(PMe_3)_2$, and then $Me_3SnSnMe_3$ (1.28 g, 3.91 mmol) was added to the solution. After 5 h of stirring at room temperature, all of the volatiles were evaporated and pentane (10 mL) was added to the residue. After the insoluble material was removed by filtration, yellow crystals were precipitated at −70 °C and washed with cold (−70 °C) pentane (3 × 5 mL). The product was dried in vacuo and collected in a glovebox. Yield: 54% (0.596 g). Anal. Calcd for $C_{12}H_{36}P_2PdSn_2$: C, 24.59; H, 6.19. Found: C, 24.86; H, 6.40.

Preparation of 3b. 3b was obtained similarly using $Pd(styrene)(PMePh_2)_2$, which was prepared in situ from $PdEt_2(PMePh_2)_2$ and styrene with stirring at room temperature for 3 h. Yield (yellow crystals): 54% (1.25 g). Anal. Calcd for $C_{32}H_{44}P_2PdSn_2$: C,46.06; H, 5.30. Found: C, 45.68; H, 5.22.

X-ray Structure Determination of 2a. Suitable crystals for diffraction studies were grown by slow diffusion of hexane into a toluene solution of **2a** at room temperature. A single crystal mounted on a glass fiber with grease was put in a cold nitrogen stream. Intensity data were collected on a Rigaku AFC7R four-circle diffractometer. A Rigaku XR-TCS-2-050 temperature controller was used. The cell dimensions were determined by least-squares refinement of diffractometer angles for 25 automatically centered reflections. The structure was solved and refined using the teXsan crystallographic software package on an IRIS Indigo computer. Scattering factors for neutral atoms were from Cromer and Waber,[20] and anomalous dispersion[21] was used. The positions of the heavy atoms were

(20) Cromer, D. T.; Waber, J. T. In *International Tables for X-ray Crystallography*; The Kynoch Press: Birmingham, England, 1974; Vol. IV.

determined by direct methods SHELXS86.[22] The platinum atom is on a crystallographic 2-fold axis. The structure was expanded by DIRDIF[23] and refined with full-matrix least-squares. The weighting scheme was $w = [\sigma^2(F_o) + 0.0001\ F_o^2]^{-1}$. An empirical absorption correction based on three azimuthal scans[24] was applied. The final least-squares cycle included non-hydrogen atoms with anisotropic thermal parameters and hydrogen atoms at fixed positions with isotropic thermal parameters which were 1.2 times those of the connected atoms. The crystal data and a description of the structure refinement are summarized in Table 3.

X-ray Structure Determination of 3a. Single crystals were obtained by slow cooling of a pentane/toluene solution of **3a**. The data collection method was similar to that for **2a**. The positions of the heavy atoms were determined by direct methods, SHELXS86. The structure was expanded by DIRDIF and refined with full-matrix least-squares. The weighting scheme was $w = [\sigma^2(F_o) + 0.0001\ F_o^2]^{-1}$. An empirical absorption correction, DIFABS,[25] was applied. The final least-squares cycle included non-hydrogen atoms with anisotropic thermal parameters. The crystal data and a description of the structure refinement are summarized in Table 3.

Acknowledgment. This work was supported in part by a Grant-in-Aid for Scientific Research on Priority Areas (Grant No. 09239104) from the Ministry of Education, Science, Sports, and Culture, Japan. The authors are grateful to Dr. Yasushi Obora for helpful discussions.

Supporting Information Available: Tables of crystal data and refinement details, atomic coordinates, thermal parameters, bond distances, bond angles, and torsion angles and ORTEP diagrams of **2a** and **3a** (15 pages). Ordering information is given on any current masthead page.

OM970957J

(21) Creagh, D. C.; McAuley, W. J. In *International Tables for X-ray Crystallography*; A. J. C. Wilson, Ed.; Kluwer Academic Publishers: Boston, 1992; Vol. C, p 219.

(22) Sheldrick, G. M. In *Crystallographic Computing 3*; Sheldrick, C. K. G. M., Goddard, R., Eds.; Oxford University Press: Oxford, 1985; p 175.

(23) Parthasarathi, V.; Beurskens, P. T.; Slot, H. J. B. *Acta Crystallogr.* **1983**, *A39*, 860.

(24) North, A. C. T.; Phillips, D. C.; Mathews, F. S. *Acta Crystallogr.* **1968**, *A24*, 351.

(25) Walker, N.; Stuart, D. *Acta Crystallogr.* **1983**, *A39*, 158.